Contrib Mineral Petrol (2001) 140: 554–566
DOI 10.1007/s004100000211

F. Bea · A. Arzamastsev · P. Montero · L. Arzamastseva

Anomalous alkaline rocks of Soustov, Kola: evidence of mantle-derived metasomatic fluids affecting crustal materials

Received: 5 May 2000 / Accepted: 29 September 2000 / Published online: 1 December 2000

Abstract The intrusive complexes of Gremiakha-Vyrmes and Soustov represent the two extremes of the Early Proterozoic alkaline plutons of Kola, predominantly composed of feldespathoidal syenites. Gremiakha-Vyrmes rocks (zircon age: 1,884 ± 6 Ma) have trace-element and isotope signatures ($^{87}Sr/^{86}Sr_t \approx 0.704$, $\epsilon Nd_t \approx -3$–1.3) compatible with an ultimate mantle origin. Soustov syenites (zircon age: 1,872 ± 8 Ma) are totally different and show an acute crustal imprint. They have sodaline and analcite instead of nepheline, contain a plethora of REE-HFSE-rich accessories, and are characterised by elevated contents of F, Cl, REE, Y, Th, U, Zr, Hf, Nb, Ta, Sn, Be, Li, Rb, Tl, Pb and Cs, negative Eu anomalies, K/Rb ≈ 190–160, Nd/Th ≈ 3, and Nb/Ta ≈ 12, with extremely high $^{87}Sr/^{86}Sr_t$ (> 0.720) and, at the same time, relatively high ϵNd_t (≈−1.6–1.7). In this paper, we explore the idea that the anomalous features of Soustov syenites can be explained if we assume they are derived from a metasomatic agent, initially an H_2O-CO_2 supercritical fluid released by alkaline mafic magmas, that was profoundly contaminated during percolation through crustal materials. As percolation advanced, the bulk composition of the fluid solute changed from alkali halides and carbonates to a silica-undersaturated alkaline melt. When the fluid cooled to a temperature of ∼550–600 °C, it reached the point at which vapor and melt were no longer miscible and split into two components, a vapour phase and a Cl- and F-rich silica-undersaturated silicate melt that crystallised to produce Soustov syenites. To study this process, we have developed a numerical method for modelling the solute composition of the fluid during the infiltration metasomatism. Our results, using the LREE abundances and the Sr and Nd isotope composition of a Gremiakha-Vyrmes pegmatite as the starting solute composition of the fluid, and the mode and mineral trace-element and isotope composition of a common Kola gneiss as representative of percolated materials, indicate that the fluid would have acquired a signature closely matching Soustov's, even in the case of Nd isotopes, if the gneiss age is 2.9 Ga, near its real age. This model is still a mere working hypothesis that needs further refinements, but may represent a reasonable explanation of the genesis of anomalous alkaline rocks with high $^{87}Sr/^{86}Sr_t$ and $\epsilon Nd_t \geq 0$, either saturated or undersaturated, which are difficult to understand in terms of magmatic fractionation/contamination.

F. Bea (✉) · P. Montero
Department of Mineralogy and Petrology,
Fuentenueva Campus, University of Granada,
18002 Granada, Spain
e-mail: fbea@goliat.ugr.es
Tel.: +34-95-8246176; Fax: +34-95-8243368

A. Arzamastsev · L. Arzamastseva
Geological Institute, Kola Science Center,
14 Fersman St, Apatity, Murmansk region, 184200 Russia

Introduction

In the Kola Peninsula, the Early Proterozoic (∼1,900 Ma) episode of alkaline magmatism produced numerous small complexes, with feldspathoidal syenites often predominating (Kukharenko et al. 1971; Mitrofanov et al. 1995). The syenites from these complexes share similar major-element and Nd isotope compositions ($\epsilon Nd_t \approx -3$–2), but show stunning differences in trace elements and Sr isotopes (Tables 1, 2). In most cases, they have $^{87}Sr/^{86}Sr_t \approx 0.704$ and element ratios consistent with an ultimate mantle origin. In a few cases, however, such those of Soustov and the plutono-volcanic complexes of Tominga (Batieva et al. 1983) or Poritash mountain (Balashov 1996), the syenites and trachytes have notably high $^{87}Sr/^{86}Sr_t$ (up to 0.720) and distinctive trace-element patterns, with low K/Rb, low Nd/Th, low Nb/Ta, negative Eu anomalies, etc., which reveal an acute crustal imprint. These features, especially the simultaneously high $^{87}Sr/^{86}Sr_t$ and $^{143}Nd/^{144}Nd_t$, cannot have been caused merely by the bulk incorporation of crustal materials into mantle-derived melts.

Table 1 Major- and trace-element composition of Soustov and Gremiakha-Vyrmes syenites. Associations: *Foidolitic; **ultramafic; ***silica-saturated peralkaline

	Soustov							Gremiakha-Vyrmes							
	1	2	3	4	5	6	7	2*	3*	5**	6***	7*	14*	15**	16**
Major-element composition (%)															
SiO_2	63.27	61.21	57.23	62.30	57.48	56.04	56.20	52.58	55.80	57.53	63.79	55.68	56.39	59.23	60.86
TiO_2	0.17	0.23	0.29	0.14	0.51	0.29	0.28	0.85	0.40	1.02	0.48	0.50	0.32	1.08	0.52
Al_2O_3	19.72	19.17	19.51	18.90	15.71	17.66	20.32	22.75	21.90	15.62	16.22	16.24	19.98	16.05	17.40
Fe_2O_3	1.22	2.23	2.44	1.09	4.27	2.90	2.11	2.58	1.42	3.63	2.35	4.88	2.33	4.04	2.28
FeO	1.58	2.45	3.74	1.25	5.09	3.32	2.92	2.63	2.84	6.58	3.32	2.79	3.72	5.23	2.74
MgO	0.12	0.12	0.46	0.03	1.51	0.72	0.19	0.77	0.40	0.52	0.13	0.59	0.41	0.45	0.22
MnO	0.06	0.13	0.18	0.06	0.26	0.15	0.16	0.09	0.10	0.28	0.13	0.17	0.14	0.24	0.11
CaO	0.96	1.21	2.13	0.67	2.81	3.06	1.32	1.87	1.12	2.73	1.16	3.10	1.56	3.21	2.53
Na_2O	6.55	7.14	7.33	7.63	6.58	10.09	7.70	10.39	8.97	6.10	7.03	7.70	7.51	6.13	6.87
K_2O	6.15	5.54	5.25	5.64	5.06	4.58	6.23	5.19	5.53	3.88	4.97	5.54	5.15	3.95	4.40
P_2O_2	0.03	0.03	0.05	0.03	0.09	0.05	0.05	0.11	0.08	0.22	0.12	0.11	0.11	0.27	0.19
F	0.16	0.11	0.29	0.28	0.39	0.21	0.32	≤ 0.06	≤0.06	≤ 0.06	≤0.06	≤ 0.06	≤0.06	≤ 0.06	≤ 0.06
Cl	0.36	0.29	0.39	0.41	0.47	0.31	0.42	≤ 0.03	≥30.03	≤ 0.03	≤0.03	≤ 0.03	≤0.03	≤ 0.03	≤ 0.03
H_2O	0.17	0.33	0.93	1.64	0.24	0.71	1.72	0.32	1.35	1.54	0.17	2.56	1.95	0.11	0.89
Total	100.52	100.18	100.21	100.07	100.47	100.09	99.94	100.14	99.97	99.68	99.90	99.91	99.60	100.00	99.06
Trace-element composition (ppm)															
Li	47	99	105	69	51	151	73	4.1	14.4	7.07	12.7	4.10	20.4	4.9	3.2
Rb	276	325	302	247	273	217	369	81.0	76.2	23.7	84.9	89.9	116	16.5	14.8
Cs	5.13	5.88	8.75	4.12	8.13	4.26	10.7	0.31	0.62	0.45	0.48	0.95	1.28	0.20	0.25
Be	5.07	14.0	13.3	5.64	8.78	11.1	19.2	3.72	2.04	0.53	3.95	3.39	1.58	0.30	0.38
Sr	130	171	608	83.5	86.1	217	425	755	198	103	164	1240	221	114	129
Ba	200	173	396	172	150	291	112	2059	578	6870	434	1586	223	6899	11960
Sc	0.25	0.76	0.94	0.03	3.16	2.96	0.64	2.37	1.51	10.02	2.07	3.62	1.90	14.3	9.98
V	1.12	0.83	5.37	0.47	1.12	0.99	4.89	23.2	1.43	1.84	1.19	16.5	1.24	0.69	0.53
Cr	2.57	1.32	120	0.47	36.6	7.99	17.6	23.1	12.3	7.14	23.2	37.1	3.16	10.43	9.86
Co	0.63	1.35	2.61	34.8	2.02	1.97	3.36	7.43	3.56	3.07	1.87	4.58	3.99	2.37	1.12
Ni	2.21	3.51	8.99	0.54	8.96	5.14	7.38	9.95	2.72	6.44	5.55	7.98	4.76	6.24	4.85
Cu	6.74	7.19	12.9	3.52	27.5	11.4	31.01	13.1	8.73	13.3	8.90	10.7	10.1	8.22	5.75
Zn	47.9	124	152	34.7	286	141	149	107	56.8	247	87.7	120	69.7	201	211
Ga	32.7	37.0	38.8	32.1	32.7	37.9	35.5	50.5	33.3	25.6	42.9	48.7	34.2	24.47	24.7
Y	26.2	62.3	79.3	32.9	45.5	62.2	42.0	5.00	7.80	7.22	18.9	8.33	9.72	5.75	4.69
Nb	56.5	159	161	67.8	138	161	123	32.3	47.4	9.28	54.9	367	95.3	4.48	4.66
Ta	5.01	12.6	13.6	6.92	9.09	13.5	9.94	2.71	1.73	1.11	2.64	15.3	3.42	0.28	0.33
Zr	361	1258	1137	363	1141	1879	783	106	33.8	58.3	322	542	81.2	21.9	41.1
Hf	7.51	27.3	25.7	8.05	29.09	43.5	17.4	3.54	1.37	1.60	7.66	15.4	2.77	0.69	1.06
Mo	0.91	4.18	3.28	2.01	5.63	6.15	10.5	0.44	0.69	1.87	1.52	0.83	0.21	0.92	0.72
Sn	3.99	13.95	15.8	4.66	6.47	15.9	15.7	0.28	0.04	0.130	0.92	8.74	0.37	0.36	0.62
Tl	0.77	0.80	0.77	0.55	1.03	0.89	1.32	0.14	0.23	0.07	0.26	0.14	1.07	0.07	0.05
Pb	11.4	27.8	32.7	20.05	8.96	28.819	24.9	2.35	2.78	3.01	3.61	6.98	4.28	2.83	2.31
U	2.55	8.45	8.39	3.18	4.02	7.49	9.3	0.34	1.74	2.20	0.88	12.4	1.19	0.11	0.14
Th	11.8	38.5	41.1	12.33	18.74	35.1	45.7	0.90	1.99	1.55	3.76	2.65	1.70	0.33	0.45
La	43.7	115	173	60.7	112	132	148	9.09	27.7	10.4	31.1	15.1	33.5	8.78	6.14
Ce	86.3	207	311	118	222	236	248	20.4	61.4	24.9	81.2	38.3	76.9	22.3	15.5
Pr	8.9	20.6	31.6	11.9	25.3	23.0	23.3	2.66	7.36	3.34	9.91	4.78	9.55	3.24	2.34
Nd	30.4	67.0	106	39.9	92.4	76.5	73.1	10.8	27.4	15.3	41.1	19.1	36.1	15.2	11.1
Sm	5.46	11.5	18.3	7.06	16.5	13.2	11.1	2.21	5.51	3.34	8.60	3.70	6.49	3.25	2.58
Eu	0.78	1.35	2.42	0.92	2.14	1.61	1.19	0.78	1.37	5.53	2.29	1.34	1.41	6.14	4.62
Gd	4.46	9.44	14.31	5.78	12.1	10.1	8.74	1.67	3.38	2.70	6.53	2.88	4.56	2.70	2.03
Tb	0.75	1.60	2.32	1.01	1.72	1.66	1.39	0.21	0.42	0.35	0.89	0.41	0.54	0.32	0.27
Dy	4.60	9.99	13.18	5.73	9.52	9.91	7.76	0.92	1.97	1.66	4.51	1.99	2.62	1.46	1.20
Ho	1.00	2.17	2.77	1.25	1.89	2.21	1.47	0.15	0.34	0.29	0.80	0.37	0.44	0.23	0.21
Er	2.63	6.10	7.26	3.16	4.63	6.26	3.70	0.36	0.74	0.69	1.91	0.85	0.92	0.53	0.44
Tm	0.37	0.90	1.06	0.41	0.73	0.98	0.55	0.05	0.09	0.10	0.25	0.14	0.12	0.07	0.06
Yb	1.83	4.91	5.49	2.13	4.32	5.52	3.06	0.34	0.53	0.52	1.62	0.90	0.76	0.43	0.34
Lu	0.22	0.69	0.76	0.26	0.71	0.84	0.42	0.06	0.08	0.09	0.26	0.16	0.11	0.07	0.06

Rather, they suggest a complex open-system interaction between old crustal materials and mantle-derived alkaline fluids, either a melt or a supercritical hydrous fluid.

The aim of this report is to decipher the mechanism(s) by which such anomalous syenites could have been generated. For this purpose, we have compared the mineralogy, geochemistry and Sr and Nd isotope geology of two massifs, Soustov and Gremiakha-Vyrmes (Fig. 1). They are presumably coeval and represent the two extremes of the compositional spectrum of the Early

Table 2 Sr and Nd isotope of Soustov (*SO*) syenites, the tonolitic gneiss used for modeling (*SU-19*) and Gremiakha-Vyrmes (*GV*) rocks. Identification numbers are the same as in Table 1

	Rb (ppm)	Sr (ppm)	$^{87}Rb/^{86}Sr$	$^{87}SR/^{86}Sr$	$^{87}SR/^{86}Sr$ (1,880 Ma)	eSr (1,880 Ma)	Nd (ppm)	Sm (ppm)	$^{147}Sm/^{144}Nd$	$^{143}Nd/^{144}Nd$	$^{143}Nd/^{144}Nd$	eNd (1,880 Ma)
SO-1	276	130	6.262	0.885483	0.716066	196	30.4	5.46	0.1086	0.511481	0.510138	−1.304
SO-2	325	171	5.593	0.872685	0.721358	271	67.0	11.5	0.1040	0.511464	0.510178	−0.521
SO-3	302	608	1.443	0.759940	0.720905	265	106	18.3	0.1036	0.511574	0.510293	1.724
SO-4	247	83.5	8.745	0.954790	0.718197	226	39.9	7.06	0.1069	0.511446	0.510124	−1.588
SO-5	273	86.1	9.429	0.975213	0.720107	253	92.4	16.5	0.1082	0.511625	0.510287	1.609
SO-6	217	217	2.915	0.797171	0.718302	227	76.5	13.2	0.1040	0.511469	0.510182	−0.437
SO-7	369	425	2.536	0.791956	0.723346	299	73.1	11.1	0.0917	0.511312	0.510178	−0.522
SUB-19	76.1	760	0.290	0.717163	0.709318	100	4.02	16.6	0.1494	0.511997	0.510148	−1.109
GV-1	49.7	812	0.177	0.707162	0.702372	1.13	45.9	9.62	0.1268	0.511841	0.510272	1.324
GV-2	81.0	755	0.311	0.712491	0.704088	25.5	10.8	2.21	0.1235	0.511745	0.510217	0.248
GV-3	76.2	198	1.118	0.735494	0.705246	42.0	27.4	5.51	0.1215	0.511430	0.509927	−5.432
GV-4	79.7	266	0.867	0.725758	0.702288	−0.06	17.1	3.05	0.1075	0.511558	0.510228	0.462
GV-5	23.7	103	0.667	0.723143	0.705092	39.8	15.3	3.34	0.1319	0.511783	0.510152	−1.039
GV-6	84.9	164	1.504	0.744119	0.703438	16.3	41.1	8.60	0.1265	0.511709	0.510143	−1.198
GV-7	89.9	1240	0.210	0.708997	0.703319	14.6	19.1	3.70	0.1173	0.511712	0.510261	1.098
GV-8	76.0	65.3	3.396	0.795050	0.703163	12.3	7.60	2.32	0.1844	0.512330	0.510049	−3.059
GV-9	59.1	247	0.693	0.722267	0.703518	17.4	35.6	7.04	0.1194	0.511635	0.510158	−0.917
GV-10	10.4	976	0.031	0.704752	0.703921	23.2	29.7	6.77	0.1377	0.511862	0.510159	−0.897
GV-11	0.14	16.1	0.026	0.704558	0.703865	22.4	0.94	0.21	0.1361	0.511788	0.510104	−1.980
GV-12	4.20	783	0.016	0.704311	0.703891	22.7	58.6	13.1	0.1348	0.511797	0.510130	−1.469
GV-13	4.29	841	0.015	0.704345	0.703946	23.5	37.6	8.59	0.1382	0.511837	0.510127	−1.517

Proterozoic alkaline magmatism of Kola, highly anomalous in the case of Soustov and derived from nearly pure mantle melts in the case of Gremiakha-Vyrmes. We have verified that both massifs are the same age by dating them with the single-zircon stepwise-evaporation $^{207}Pb/^{206}Pb$ and whole-rock Rb-Sr methods. To model the variations of trace elements and isotope ratios during infiltration metasomatism, we have developed a numerical method enabling us to propose a percolation mechanism capable of producing the anomalous chemical and isotopic signature of the Soustov rocks.

Geological setting

The Gremiakha-Vyrmes Complex

The Gremiakha-Vyrmes Complex (Fig. 1) is located within the Kola-Norwegian part of the Central Kola terrane, inside the N-S fault zone separating Pechenga from the Imandra-Varzuga regions. It comprises three rock associations characterised by the presence of ultrabasic rocks, foidolitic basic and intermediate rocks, and peralkaline silica-saturated and oversaturated rocks. The ultrabasic association is composed of peridotites, pyroxenites, gabbros and anorthosites with minor feldspathoid-bearing syenites and monzodiorites. The foidolitic association consists of melteigites, ijolites, juvites and nepheline syenites. The foidolites form a stratified body, with alternating layers of melanocratic and leucocratic varieties. Nepheline syenites, either agpaitic or miaskitic, define a net of veins cross-cutting the foidolites. They usually consist of foyaites that may locally grade into foyaitic pegmatites or alkaline syenites (Kukharenko et al. 1971). The peralkaline silica-saturated association forms a body in the north of the massif composed of peralkaline granite and syenites, rarely feldspathoidal, with a mafic mineralogy consisting either of aegirine-arfvedsonite, aegirine-aenigmatite, or aegirine-richterite.

The Soustov intrusion

The Soustov Intrusion lies in the vicinity of the southern contact of the giant Devonian agpaitic complex of Khibina, within the axial zone of the Imandra-Varzuga volcanic belt (Fig. 1). It is a lens-shaped 2 × 10-km body whose contacts are roughly parallel to the southern boundary of Khibina. The Soustov Intrusion is composed almost exclusively of syenites that, in most cases, are feldspathoidal and peralkaline. Non-feldspathoidal syenites are sparse, and a narrow rim of quartz syenite forms the contact zone with the country rock.

Analytical methods

Whole-rock major-element determinations were performed by X-ray fluorescence after fusion with lithium tetraborate. Typical precision was better than ±1.5% for an analyte concentration of 10 wt.%. Trace-element determinations were done by ICP-mass spectrometry (ICP-MS) with a Perkin Elmer Elan-5000 spectrometer using Rh as internal standard. Precision was better than ±2% and ±5% for analyte concentrations of 50 and 5 ppm, respectively. Samples for Sr and Nd isotope analyses were digested in a clean room using ultra-clean reagents and analysed by thermal ionization mass spectrometry (TIMS) in a Finnigan Mat 262 spectrometer after chromatographic separation with ion-exchange resins. Normalisation values were $^{86}Sr/^{88}Sr = 0.1194$ and $^{146}Nd/^{144}Nd = 0.7219$. Blanks were 0.6 and 0.09 ng for Sr and Nd, respectively. The external precision (2σ), estimated from the analysis of ten replicates of the standard WS-E (Govindaraju et al. 1994), was

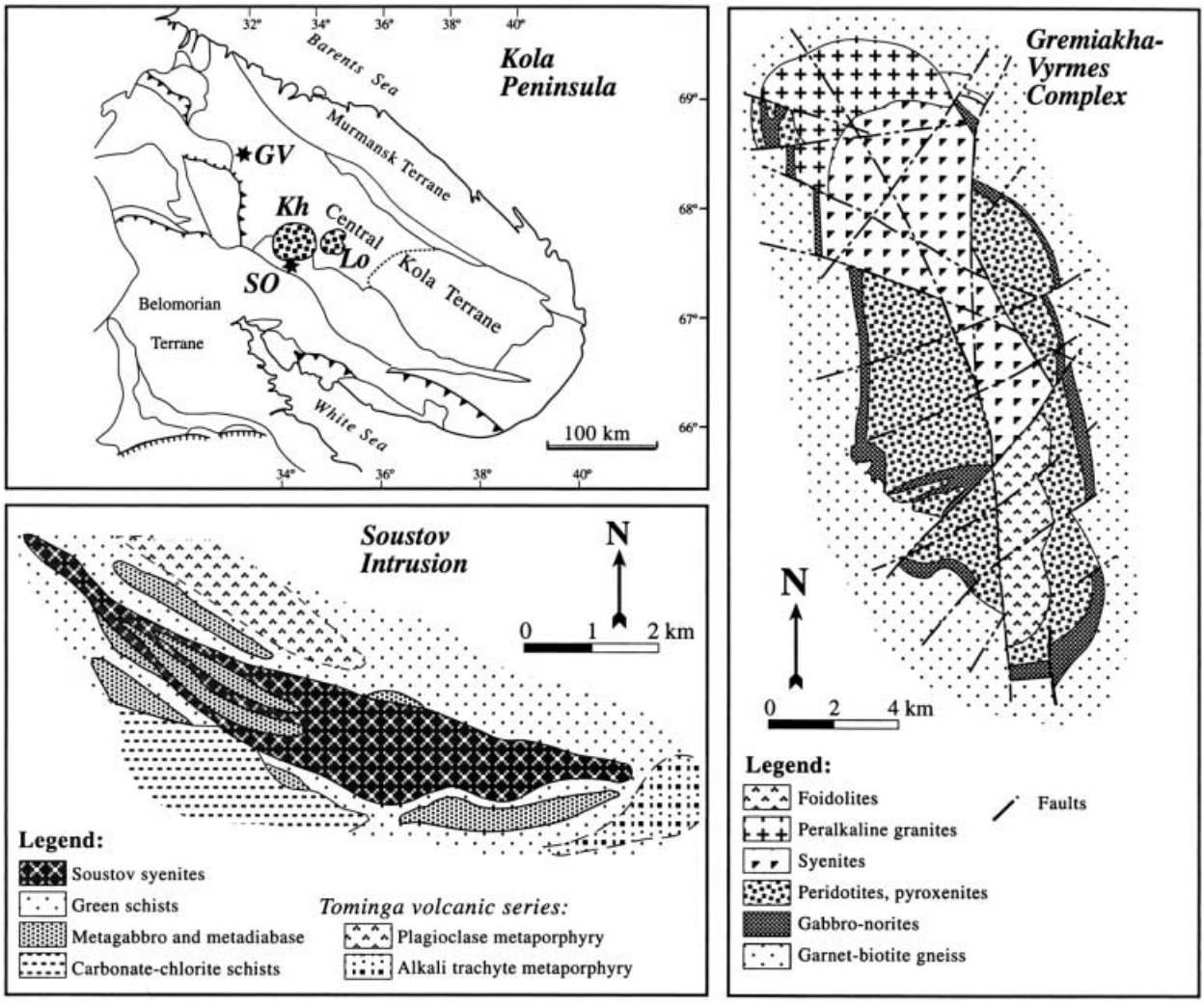

Fig. 1 Location and schematic maps of Gremiakha-Vyrmes (*GV*) and Soustov (*SO*). The giant Palaeozoic massifs of Khibina (*Kh*) and Lovozero (*LV*) are also shown

better than 0.003% for $^{87}Sr/^{86}Sr$, and 0.0015% for $^{143}Nd/^{144}Nd$. $^{87}Rb/^{86}Sr$ and $^{147}Sm/^{144}Nd$ were directly determined by ICP-MS (Montero and Bea 1998), with a precision, estimated by analysing ten replicates of the standard WS-E, better than 1.2% and 0.9% (2σ) respectively.

Major-element analyses of minerals were obtained by wavelength dispersive analyses with a Camebax SX-50 electron microprobe using synthetic standards. Accelerating voltage was 20 kV and beam current was 15 nA. Coefficients of variation were close to ±1%, ±2.5%, and ±5% for 10 wt.%, 1 wt.%, and 0.25 wt.% analyte concentrations, respectively. REE analyses of accessories were done by electron microprobe using synthetic standards. Precision was close to ±4% for 1 wt.% conc. and ±10% for 0.25 wt.% conc. REE analyses of major minerals were performed by LA-ICP-MS with a precision close to ±5% and ±10% for 50 ppm and 1 ppm, respectively (Bea et al. 1996).

Zircons were dated with the single-grain stepwise-evaporation $^{207}Pb/^{206}Pb$ method developed by Kober (1986). Lead was collected on the ionization filament for 20–30 min and then analysed in five blocks with seven scans per block. Data acquisition was performed in dynamic mode (peak hopping), using a secondary electron multiplier (SEM) as detector with the 206–204–206–207–208 mass sequence. The mass-ratio 204/206 was monitored to detect and, if necessary, correct for common lead, whose composition was calculated from the model of Stacey and Kramers (1975). Mass fractionation was corrected by multiplying by $\sqrt{(207/206)}$. Standard errors for each step were calculated according to the formula: $SE = 2^*\sigma/\sqrt{n}$. However, the 2σ confidence interval for the final age is given by $[X - t_{(0.025)}\sigma/\sqrt{n},\ X + t_{(0.025)}\sigma/\sqrt{n}]$, where X and σ are the average and standard deviation of measured steps, n the number of steps, and $t_{(0.025)}$ is the upper (0.025) point of the t distribution for n–1 degrees of freedom.

Isotopic dating

Previous age determinations of the Gremiakha-Vyrmes Complex range from 1,865 ± 45 Ma (Puskharev 1990) to 1,930 ± 52 Ma (Kukharenko et al. 1971). A recent Pb/Pb isochron in apatites yielded 1911 ± 87 Ma (Savatenkov et al. 1998). For this study, we analysed ten zircon grains with the Kober method, six from a syenite of the foidolitic association and four from a syenite of the peralkaline association, which yielded a mean age of 1,884 ± 6 Ma (Table 3; Fig. 2). Fourteen samples from the three main facies, including peridotites, ijolites, nepheline syenites and peralkaline granitoids, fit well into a $^{87}Sr/^{86}Sr$ vs $^{87}Rb/^{86}Sr$ regression line with a slope corresponding to 1,870 Ma and an intercept on the y

Table 3 Single-zircon stepwise evaporation data of zircons from Gremiakha-Vyrmes and Soustov

Zircon	$^{204}Pb/^{206}Pb$	$^{207}Pb/^{206}Pb$	$^{204}Pb/^{206}Pb$ (corrected)	Error (2s%)	Age (Ma)
	Gremiakha-Vyrmes				
1	0.000643	0.123233	0.114835	0.28	1,877 ± 5
2	0.000647	0.124358	0.115645	0.34	1,890 ± 6
3	0.000658	0.124127	0.115269	0.21	1,884 ± 4
4	0.000658	0.124115	0.115250	0.13	1,884 ± 3
5	0.000646	0.124908	0.116216	0.22	1,899 ± 4
6	0.000355	0.118926	0.114416	0.29	1,871 ± 6
7	0.000653	0.123944	0.115420	0.29	1,886 ± 5
8	0.000242	0.118530	0.116373	0.16	1,888 ± 3
9	0.000397	0.119959	0.114885	0.59	1,878 ± It
10	0.000662	0.123763	0.115119	0.41	1,882 ± 8
Mean					1,884 ± 6
	Soustov				
1	0.000019	0.113938	0.113959	0.82	1,863 ± 15
2	0.000035	0.114748	0.114558	0.36	1,873 ± 7
3	0.000087	0.115871	0.114979	0.43	1,879 ± 8
4	0.000071	0.115378	0.114696	0.28	1,875 ± 5
5	0.000459	0.120418	0.114228	0.35	1,868 ± 7
Mean					1,872 ± 8

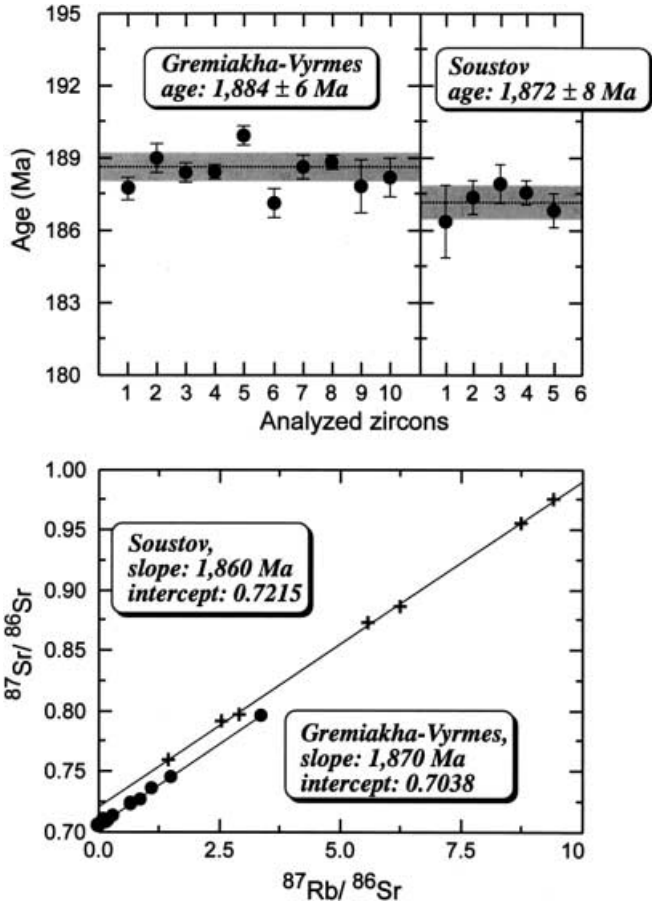

Fig. 2 Single-zircon stepwise $^{207}Pb/^{206}Pb$ ages and Sr isotope evolution diagram for Soustov and Gremiakha-Vyrmes rocks. Note that the age is virtually identical, but Soustov rocks have a much higher initial $^{87}Sr/^{86}Sr$

axis of $^{87}Sr/^{86}Sr = 0.7038$ (Table 2; Fig. 2). We thus consider the zircon age of 1,884 ± 6 Ma to represent the best estimate for the crystallisation age of the Gremiakha-Vyrmes Complex.

The only previous chronological data of Soustov were a discordant zircon age of 1,745 Ma and a $^{87}Rb/^{86}Sr$ vs $^{87}Sr/^{86}Sr$ regression line with poorly fitting samples that yielded 2,000 Ma, with $^{87}Sr/^{86}Sr_{2,000\ Ma}$ showing a high dispersion, from 0.701 to 0.719 (Batieva et al. 1983). We have analysed five zircon grains which yielded a mean age of 1,872 ± 8 Ma, slightly younger than in the case of Gremiakha-Vyrmes (Table 3; Fig. 2). In the Sr isotope evolution diagram (Table 2; Fig. 2), seven whole-rock samples fit into a regression line with a slope corresponding to 1860 Ma and an intercept on the *y* axis of $^{87}Sr/^{86}Sr = 0.7215$, a value notably higher than in the case of Gremiakha-Vyrmes.

Our zircon data show, therefore, that the Gremiakha-Vyrmes and Soustov bodies formed within a narrow interval of ~12 Ma, so that we can safely assume they belong to the same magmatic episode.

Mineralogy and petrography of syenites

Gremiakha-Vyrmes

The three rock associations of Gremiakha-Vyrmes include syenites. Those belonging to the foidolitic association are either agpaitic or miaskitic foyaites, with nepheline as the only feldspathoid and albite as the dominant feldspar. The mafic assemblage is composed of tschermakitic aegirine-augite, hastingsitic amphibole, and annitic biotite. Amphibole and biotite usually replace early crystals of clinopyroxene. The accessory assemblage is composed of Mn-rich ilmenite, titanite, apatite, zircon, rare baddeleyite, abundant crystals of a

Si-Ti-Fe-Ba mineral (benitoïte?), barite, and rare but conspicuous celestine. The only REE-saturated minerals found under the SEM are scarce crystals of metamictic Ca-poor allanite.

The syenites from the ultramafic association are orthoclase-rich pulaskites and akerites, infrequent syenogabbros, with rare or no nepheline. The mafic association is formed of fayalite, ferropargasite, ferrian hedenbergite and annitic biotite. The accessory assemblage comprises abundant magnetite that forms simplectitic intergrowths with ferrian hedenbergite, ilmenite, apatite, zircon and rare barite. So far, we have found no REE-saturated minerals.

The syenites from the saturated peralkaline association have very rare or no feldspathoids. The major mineral assemblage is composed of albite, microperthite, aegirine and alkaline amphibole, either riebeckite, arfvedsonite, or richterite, sometimes accompanied by aenigmatite. The accessory assemblage consists of ilmenite, apatite, zircon and rare barite. As REE-saturated accessories, they have rare crystals of a primary-appearing Ti-LREE-Ca mineral (knopite?) and more abundant crystals of a secondary-appearing LREE-Ca carbonate, sometimes with elevated Sr contents (khanneshite?).

Soustov

Soustov syenites, in contrast to Gremiakha-Vyrmes syenites, have sodalite and analcite, probably secondary, instead of nepheline. The dominant minerals are alkali feldspars, albite and microperthite accompanied by subordinate amounts of aegirine, katoforite, annitic biotite, and Ti-rich andraditic garnet. Secondary muscovite is also found locally, replacing microperthite. The accessory assemblage is by far more abundant and varied than in the Gremiakha-Vyrmes syenites. It consists of fluorite, magnetite, titanite, apatite, zircon, minor baddeleyite, allanite, LREE-Ca silicates (kaynosite?), LREE-Nb-silicates (nacareniobsite?), LREE-Al-silicates (allumobrittolite?), Y-HREE-silicates (thalenite?), LREE-carbonates (parisite and bastnaesite), thorite, pyrochlore, cheralite, chalcopyrite, galena and barite. Most of these minerals, especially the REE-rich accessories, have textures indicating crystallisation during late-magmatic conditions.

Geochemistry

Major and trace elements

The syenites of both massifs have a similar major-element composition, except for the much higher F and Cl but slightly lower P_2O_5 and TiO_2 of the Soustov syenites (Table 1). In both cases, they consist of intermediate rocks with total alkalis in the range of 10–16 wt.% (Fig. 3), $Na_2O > K_2O$, and an agpaitic index

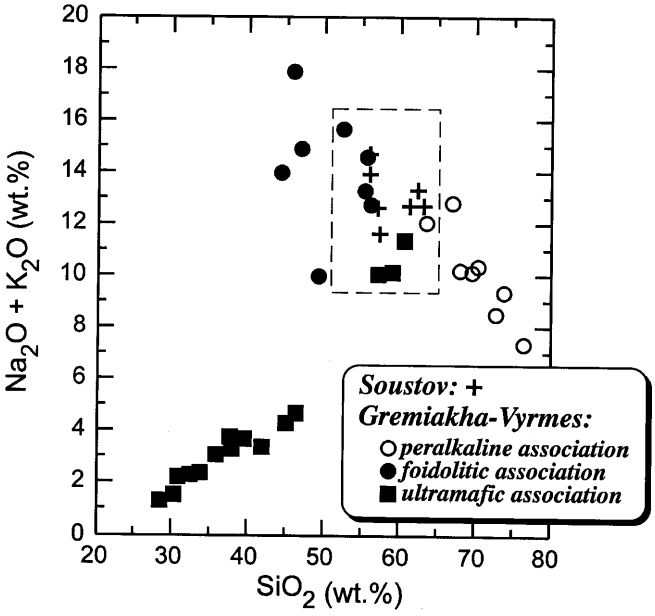

Fig. 3 Total-alkalis vs silica diagram of Soustov and Gremiakha-Vyrmes rocks. The *dashed rectangle* encloses the syenites of both massifs

(AI = mol $Na_2O + K_2O/Al_2O_3$) close to 1. Soustov syenites are always silica-undersaturated, but Gremiakha-Vyrmes syenites, especially those related to the peralkaline granitoids, can also be saturated or slightly oversaturated (Table 1).

Apart from the notorious differences in halogens, the syenites of both massifs show a marked contrast in their trace-element composition (Table 1). Soustov syenites are approximately five to ten times richer in LREE, HREE, Y, Th, U, Zr, Hf, Nb, Ta, Sn, Be, Li, Rb, Tl, Pb and Cs, but considerably poorer in Ba and, to a lesser extent, in Sr, V and Sc. Their chondrite-normalised REE patterns decrease steeply from La to Sm, have a pronounced negative Eu anomaly, and then decrease gradually from Gd to Lu (Fig. 4).

In contrast, the chondrite-normalised REE patterns of the Gremiakha-Vyrmes syenites decrease moderately from La to Sm, have a very small or no Eu anomaly, either positive or negative (except in the case of those related to the ultramafic association, which have a strong positive Eu anomaly), decrease from Gd to Er and are either flat or show a progressive enrichment from Tm to Lu (Fig. 4).

In addition to the differences in absolute abundances, there is also a remarkable contrast in some meaningful elemental ratios. In Soustov, Nd/Th it is close to 3 (Fig. 5), a value very common in crustal rocks (Bea and Montero 1999; Bea et al. 1999). The syenites and related rocks of Gremiakha-Vyrmes, in contrast, have Nd/Th > 15, as usually happens in mantle-derived rocks. In Soustov, the syenites have K/Rb ≈ 140–190 (Fig. 5), a range rarely found in rocks other than highly differentiated crustal leucogranites. Gremiakha-Vyrmes syenites, on the other hand, always have a K/Rb > 350

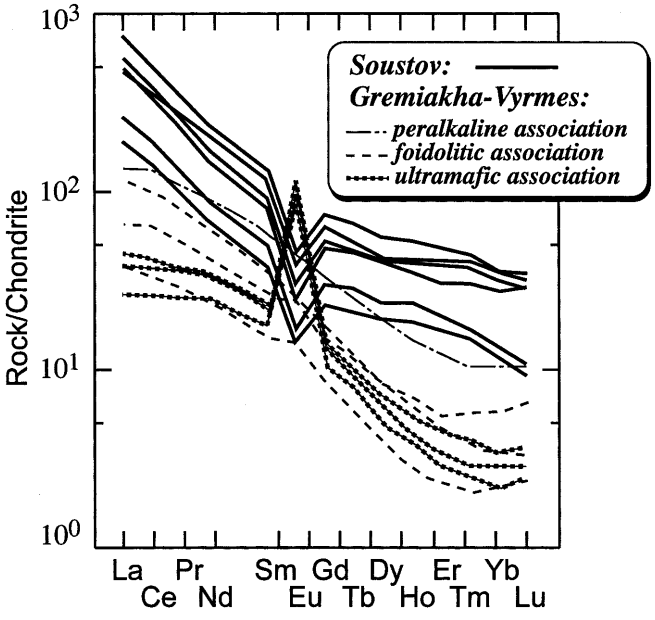

Fig. 4 Chondrite-normalized REE patterns of syenites. Note the highest REE contents and negative Eu anomaly characteristic of Soustov rocks

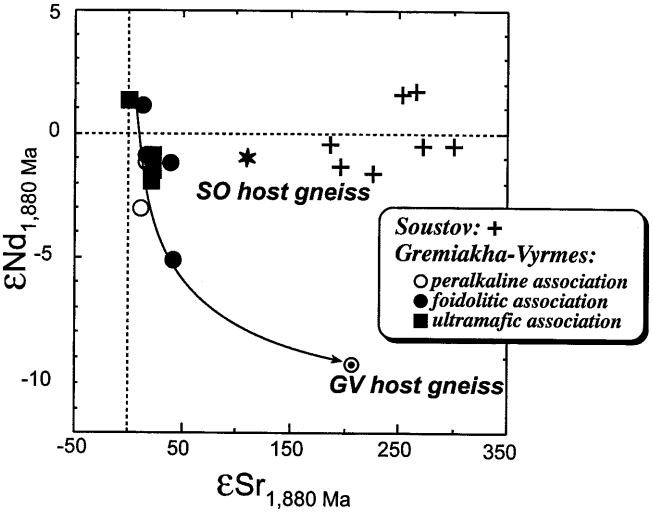

Fig. 6 $\epsilon Nd_{1,880\ Ma}$ vs $\epsilon Sr_{1,880\ Ma}$ diagram of Soustov and Gremiakha-Vyrmes massifs and their host rocks. Gremiakha-Vyrmes rocks plot into a mixing hyperbola pointed towards their host gneisses, indicating bulk assimilation. Soustov syenites, in contrast, define a weak positive correlation and do not show evidence of bulk mixing with their host rock. Data from Table 2; for Gremiakha-Vyrmes rocks, data were taken from Savatenkov et al. (1998)

(Fig. 5), reaching exceptionally high values in the syenites associated with the peridotite-gabbro complex. The average Nb/Ta ratio is close to 12 in Soustov and 22 in Gremiakha-Vyrmes, nearly matching the average crustal and mantle values, respectively (Green 1995).

We can therefore conclude that, whereas Gremiakha-Vyrmes syenites have a trace-element signature characteristic of mantle-derived magmas, Soustov syenites have many trace-element features characteristic of crust-derived magmas.

Sr and Nd Isotopes

The Sr and Nd isotope composition of Gremiakha-Vyrmes rocks is totally compatible with a mantle derivation. The initial $^{87}Sr/^{86}Sr$ is around 0.7038 and the $\epsilon Nd_{1,880\ Ma}$ ranges from −3 to 1.3 (Table 2). Both parameters are negatively correlated, defining a parabolic trend towards the host gneisses (Fig. 6) that strongly suggests bulk contamination with crustal materials.

Soustov syenites have a Nd isotope composition similar to that of Gremiakha-Vyrmes, with $\epsilon Nd_{1,880\ Ma}$ between −1.6 and 1.7, but are highly enriched in radiogenic Sr, with a $^{87}Sr/^{86}Sr_{1,880\ Ma}$ from 0.7160 to 0.7233. In contrast to Gremiakha-Vyrmes, Soustov syenites show a weak positive correlation between $\epsilon Sr_{1,880\ Ma}$ and $\epsilon Nd_{1,880\ Ma}$ (Fig. 6). Remarkably, each of these two parameters is well correlated, with a definite group of elements and meaningful interelemental ratios.

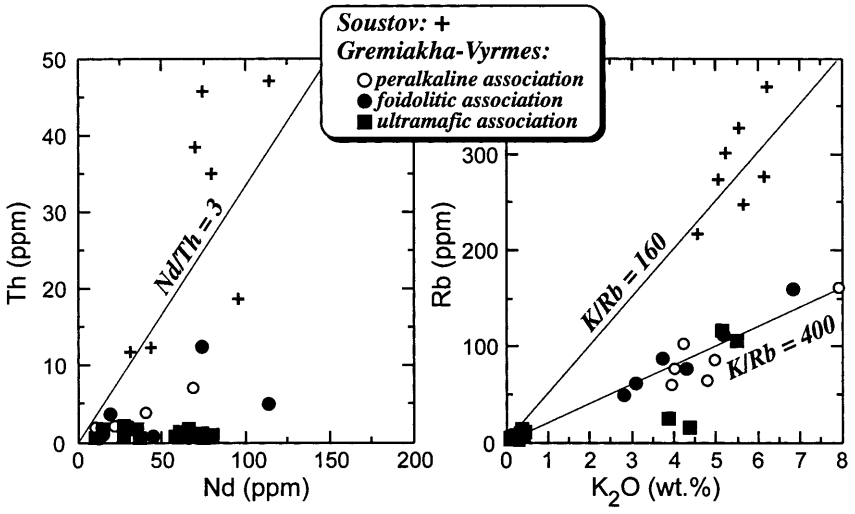

Fig. 5 Nd-Th and K-Rb ratios of rocks from Soustov and Gremiakha-Vyrmes. Whereas Gremiakha-Vyrmes rocks have mantle-like values, Soustov have values typical of continental, highly differentiated rocks (see text)

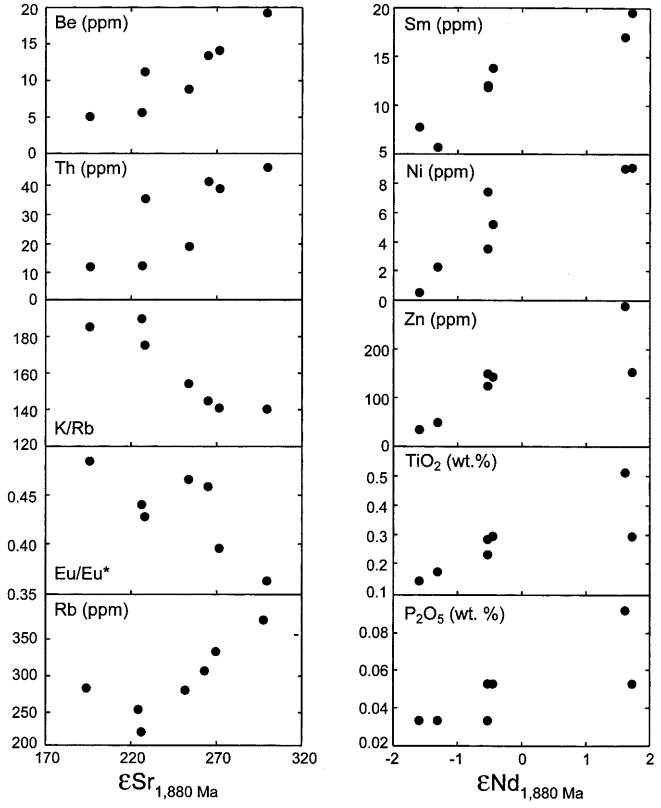

Fig. 7 $\epsilon Sr_{1,880\ Ma}$ and $\epsilon Nd_{1,880\ Ma}$ vs selected trace elements and interelemental ratios. The good correlation between $Sr_{1,880\ Ma}$ and Rb, Cs, K/Rb and Eu/Eu* is possibly caused by the simultaneous destruction of biotite and monazite. The correlation between $\epsilon Nd_{1,880\ Ma}$ and Sm, Mg, Ni, and P is related to the destruction of amphibole and apatite (see text)

$\epsilon Sr_{1,880\ Ma}$ bears a good positive correlation with elements such as Rb, Cs, Tl, Be, Pb, U, Th and the LREE, and negative with K/Rb and Eu/Eu* (Fig. 7). $\epsilon Nd_{1,880\ Ma}$ has an excellent positive correlation with the MREE, Cr, Ni, Mg, Ti, Nb, P and Nb/Ta (Fig. 7).

Discussion: a model for the genesis of Soustov syenites

To discuss the petrogenesis of the Gremiakha-Vyrmes Complex in detail is beyond the scope of this paper. For our purposes, it is enough to consider that all the available evidence points to variably fractionated mantle-derived melts that experienced limited contamination with crustal materials.

The presence of crustal components in Soustov syenites is much more evident than in the case of Gremiakha-Vyrmes, as revealed by the high proportion of radiogenic Sr, the crustal values of Nd/Th, K/Rb and Nb/Ta, and the shape of the chondrite-normalised REE patterns (Fig. 4). The presence of mantle components is, however, more difficult to recognise. Given the low values of the $\epsilon Nd_{1,880\ Ma}$ (from −1.6 to 1.7), one would expect, in theory, a significant part of the Nd currently present in Soustov syenites to have derived from the mantle, with little contribution from the crust. Nonetheless, this supposition lacks consistency with the trace-element and Sr isotope data, so that in the sections below we shall look for an alternative explanation.

The correlation between $\epsilon Nd_{1,880\ Ma}$ and $\epsilon Sr_{1,880\ Ma}$ in Soustov syenites is not negative, but weakly positive, and does not show the mixing trend towards their host gneisses depicted by Gremiakha-Vyrmes rocks (Fig. 6). It is also important to remark that the $^{87}Sr/^{86}Sr_{1,880\ Ma}$ of Soustov syenites are higher than in any other Kola rock, except in a few similar alkaline rocks. The isotopic signature of Soustov syenites, therefore, could be produced neither by assimilation nor by partial melting of crustal materials, requiring instead an open-system process able to cause a selective enrichment in radiogenic Sr.

Given the coincidence in space and time, we accept as a starting hypothesis that alkaline ultramafic magmas originating in the mantle and crystallising within the crust, such as those of the Gremiakha-Vyrmes Complex, released a metasomatic agent which first percolated through crustal materials and, once it was profoundly modified by reaction with these materials, produced the silica-undersaturated alkaline magmas of Soustov. In the paragraphs below we shall explore this idea.

Numerical modeling of trace-element and isotope ratio variations during infiltration metasomatism

The percolation of the metasomatic fluid, either a melt or an H_2O-CO_2 supercritical fluid, would have fenitised the percolated crustal materials, causing the destruction of some pre-existing minerals and the precipitation of new ones. During this process, chemical elements would have been leached from the protolith into the fluid and/or precipitated from the fluid into the newly formed minerals, the net balance depending on the composition and relative proportion of the fluid and minerals involved.

The variation in the concentration of a given trace element in the fluid with an infinitesimal increment of the percolation process is:

$$d(C_l W) = C_s dW_s + C_p dW_p; \quad (1)$$

where W, W_s and W_p, and C_l, C_s, and C_p are the masses and the element concentrations of the liquid, the phases that dissolve, and the phases that precipitate, respectively. It follows that:

$$dW = dW_s + dW_p; \quad (2)$$

$$W_s = TR_s; \quad (3)$$

$$W_p = TR_p; \quad (4)$$

where T is the mass of protolith metasomatised in each incremental step, considered as a constant, and R_s and R_p are respectively the amounts of dissolved and precipitated substances per each T mass unit of protolith.

Transforming Eq. 1 we obtain:

$$W\mathrm{d}C_l + C_l\mathrm{d}W = C_s\mathrm{d}W_s + C_p\mathrm{d}W_p; \quad (5)$$

Substituting Eq. 2 in Eq. 5 and simplifying we then have:

$$\mathrm{d}C_l = (C_s - C_l)\frac{\mathrm{d}W_s}{W} + (C_p - C_l)\frac{\mathrm{d}W_p}{W}; \quad (6)$$

Dividing both members of Eq. 6 by C_l, and substituting Eq. 3 and Eq. 4 we see that:

$$\frac{\mathrm{d}C_l}{C_l} = \frac{(C_s - C_l)}{C_l}\frac{\mathrm{d}(R_sT)}{W} + \frac{(C_p - C_l)}{C_l}\frac{\mathrm{d}(R_pT)}{W}; \quad (7)$$

Equation 7 is integrable if T is expressed as a fraction of the initial mass, W^0, of metasomatic agent. In this case we have

$$\int_{C_l^0}^{C_l}\frac{\mathrm{d}C_l}{C_l} = \frac{(C_s - C_l)}{C_l}\int_{W^0}^{W^0+W_s}\frac{R_s\mathrm{d}W}{W} + \frac{(C_p - C_l)}{C_l}\int_{W^0}^{W^0+W_s}\frac{R_p\mathrm{d}W}{W}; \quad (8)$$

and therefore

$$\ln\left(\frac{C_l}{C_l^0}\right) = \left(\frac{C_s}{C_l} - 1\right)\ln(1+TR_s) + (K-1)\ln(1 - TR_p); \quad (9)$$

where K is the solid/liquid partition coefficient for precipitating phases. C_l/C_s, however, does not represent a partition coefficient because the metasomatic agent and protolith are not in chemical equilibrium. If $R_s = 0$, the above expression is fully equivalent to Rayleigh's equation for fractional crystallisation. If there is more than one phase that precipitates or dissolves, Eq. 9 can be expressed as:

$$\ln\left(\frac{C_l}{C_l^0}\right) = \sum_1^i\left(\frac{C_s^i}{C_l} - 1\right)\ln\left(1+TR_s^i\right) + \sum_1^j\left(K^j - 1\right)\ln\left(1 - TR_p^j\right); \quad (10)$$

which can be used as long as the rates of precipitation and dissolution, the partition coefficients, and the concentration of the element in the dissolving phases remain constant.

Applications to Soustov: starting assumptions

Using Eq. 10 we have checked whether mantle-derived fluids infiltrating rocks, such as those composing the Archean crust of Kola, could acquire a geochemical signature similar to Soustov syenites. Owing to the nature of the infiltration metasomatism, there are more variables in Eq. 10 than we can determine, especially the modal fraction of phases that dissolve and precipitate. Similarly, it is unreasonable to expect the infiltrated rocks to be homogeneous in age, initial isotope composition, nature, modal fraction and composition of minerals. Therefore, the calculations that follow are not intended to be a quantitative model of how contamination during infiltration metasomatism has proceeded, but an attempt to determine whether we can simulate the chemical and isotopic anomalies of Soustov syenites starting from a set of reasonable assumptions.

For the fluid solute, we assumed a composition similar to that of the pegmatites of Gremiakha-Vyrmes (Table 4). For the solid, we assumed a composition similar to a sample of a common biotite- and amphibole-bearing TTG gneiss of Kola whose whole-rock chemical and isotopic composition, as well the trace-element composition of major and accessory minerals, has been thoroughly studied (Table 4). Based on the detailed descriptions of mineralogical changes during fenitisation of quarztfeldspathic rocks (McKie 1966; Kresten and Morogan 1986; McLemore and Modreski 1990; Sindern and Kramm 2000), we also assumed that the fenitisation process caused the total destruction of biotite and hornblende to form aegirine, alkali-amphibole and K-feldspar, and the partial albitization of the plagio-

Table 4 Parameters used in numerical modeling. **a** Solute composition of the percolating fluid (assumed to be equal to a nepheline pegmatite of Gremiakha-Vyrmes), and the mode and composition of minerals of a TTG gneiss used as protolith. The composition of minerals has been determined by LA-ICP-MS, except for allanite and monazite, which were determined by electron microprobe. The isotopic composition of minerals at 1,900 Ma has been calculated from their current Rb/Sr and Sm/Nd ratios and the isotopic composition of the gneiss SUB-19 (Table 2), $^{87}Sr/^{86}Sr_{2,900\ Ma} = 0.704972$ and $^{143}Nd/^{144}Nd_{2,900} = 0.509135$

	Fluid	Gneiss SUB-19						
		Pl	K-Fsp	Bio	Hnb	Apa	All	Mon
Modal fraction		0.49	0.04	0.14	0.10	0.003	0.00009	0.00005
Rb	35	10	150	450	25	–	–	–
Sr	965	1450	690	19	189	–	–	–
La	13.0	12.6	1.2	–	19.9	65.0	53400	132000
Ce	32.6	8.3	0.95	–	34.0	239	105000	295200
Nd	15.7	2.0	0.33	–	29.3	532	17900	13000
Sm	4.0	0.34	0.10	–	10.7	311	1890	3600
Eu	1.65	0.75	1.5	–	1.9	89	100	600
$^{87}Sr/^{86}Sr$	0.705000	0.705254	0.713838	2.540199	0.710339			
$^{143}Nd/^{144}Nd$	0.510110	0.509787	0.510329	–	0.510572	0.511434	0.509464	0.510227
b Modal fraction of minerals that dissolve and precipitate								
Dissolve		pl	K-fsp	bio	hnb	apa	all	mon
		0.15	0.00	0.14	0.1	0.003	0.00009	0.00005
Precipitate		alb	K-fsp	Na-cpx	Na-amp	tit		
		0.25	0.08	0.1	0.1	0.01		

clase; the assumed modal fraction of minerals that dissolve and precipitate is shown in Table 4.

The equilibrium distribution coefficients between alkaline fluids and minerals are virtually unknown. Therefore, we approached them empirically by analysing the albite/Na-clinopyroxene, albite/Na-amphibole, and albite/titanite concentration ratios in Soustov syenites, and the albite/whole-rock and K-feldspar/whole-rock concentration ratios in a nepheline syenite pegmatite from Miass. If we assume that mineral/whole-rock concentration ratios in the pegmatite are close to real mineral/alkaline fluid distribution coefficients, it is a simple matter to calculate a data set of distribution coefficients for all minerals involved (Table 5). The strongest point of this approach is that the mineral/mineral concentration ratios were determined in Soustov syenites; therefore, the error derived from assuming that mineral/whole-rock concentration ratios in the pegmatite represent mineral/alkaline fluid partitioning would affect all the calculated distribution coefficients in nearly the same way and so have little influence on the model (see below).

The Sr and Nd isotope composition of the protolith minerals at a given time has been calculated from the measured whole-rock isotope data and the LA-ICP-MS measured Rb/Sr and Sm/Nd ratios of minerals (Table 4); we assumed that all minerals had the same isotope composition at the moment of their formation, equal to that of the whole rock, roughly estimated at 2,900 Ma. This age implies that the crustal rocks had an age of ~1,000 Ma when they were metasomatised. For the sake of simplicity, we kept the same initial isotope composition in all models even when the age of the protolith changed.

Sr isotopes

As percolation progresses, the fluid becomes enriched in Rb and ^{87}Sr relative to ^{86}Sr, but depleted in total Sr, owing to the destruction of biotite and the precipitation of feldspars and alkali amphibole. Figure 8 shows the feasibility of infiltration metasomatism being responsible for changing the Sr isotope composition of the metasomatizing agent in a way that nearly exactly matches that displayed by Soustov syenites, if, as stated before, we assume that the metasomatic event is 1,000 Ma younger than the infiltrated rocks (Fig. 8). The calculation is quite robust, so that moderate variations in the partition coefficients and the modal fraction of intervening phases, either dissolving or precipitating, do not exert a strong influence. It is worth mentioning that, according to this model, an age difference as low as 200 Ma still can cause a perceptible enrichment in radiogenic Sr (Fig. 8). The destruction of biotite would release Rb, Cs and Tl into the fluid, thus producing the good correlation between these elements and the $^{87}Sr/^{86}Sr$. This idea gains additional support from the finding that fenites that developed from a granodiorite were progressively depleted in ^{87}Sr relative to ^{86}Sr as the intensity of the fenitisation increased (Sindern and Kramm 2000).

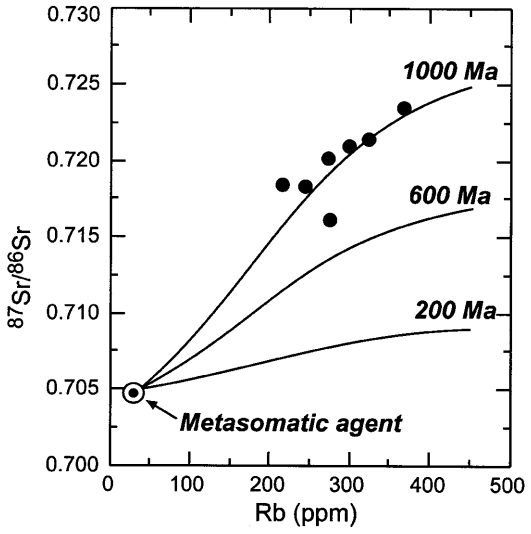

Fig. 8 Rb vs. $^{87}Sr/^{86}Sr$ paths calculated from Eq. 10 for various age differences between the metasomatic event and the percolated materials. For the assumed proportions of phases that precipitate and dissolve, the best fit is obtained for an age difference of 1,000 Ma, which corresponds to an age of 2,900 Ma for the gneiss

Table 5 Set of mineral/fluid distribution coefficients used for modeling the changes in the fluid composition during the fenitisation of the SUB-19 gneiss. Values have been calculated from albite/whole-rock and K-feldspar/whole-rock concentration ratios measured in a nepheline syenite pegmatite from Miass, and from albite/Na-clinopyroxene, albite/Na-amphibole, and albite/titanite concentration ratios measured in Soustov syenites (see text). Whole-rock analyses by solution-nebulization ICP-MS; mineral analyses by LA-ICP-MS

	Albite	K-feldspar	Aegirine	Riebeckite	Titanite
Rb	0.02	0.3	0.02	0.15	–
Sr	2.5	3.0	1.25	3.0	–
La	0.07	0.05	0.3	0.94	14.1
Ce	0.06	0.05	0.35	1.07	13.3
Nd	0.08	0.07	0.37	1.09	16.08
Sm	0.15	0.14	0.58	1.63	21.7
Eu	1.47	1.62	0.29	1.47	19.3
Gd	0.10	0.10	0.59	1.6	25.2

Rare earth elements

In crustal protoliths, the REE mainly reside in amphibole and, especially, in accessory minerals (Bea 1996), the behaviour of which during fenitisation processes is still poorly known. To appraise how the REE might behave in a process of percolation, at least qualitatively, we have built a model that, besides the destruction of amphibole, involves the dissolution of the LREE-rich accessories of the protolith, monazite, allanite and apatite (Table 4) and the simultaneous precipitation of REE-rich titanite, which seems compatible with the accessory mineralogy of fenitised granite rocks (Montero

et al. 1998). To avoid additional uncertainties arising from the behaviour of HREE-rich accessories, such as zircon, we have limited the calculations to the LREE and MREE. The results of applying Eq. 10 with the data from Tables 4 and 5 show that this model, however crude, is able to simulate a REE composition for the percolating fluids that nearly exactly matches the composition of Soustov syenites (Fig. 9), characterised by elevated LREE contents that decrease rapidly with increasing atomic number and a small negative Eu anomaly. The main contributor of LREE, Th and U to the fluid is monazite; since in the percolated gneiss a significant part of this mineral is included within biotite, both minerals are most likely leached into the fluid in the same way, thus causing a good positive correlation between $^{87}Sr/^{86}Sr$, Rb, Cs and Tl on one hand, and LREE, U, Th, and the LREE, U and Th on the other hand (see Fig. 7).

Nd isotopes

One of the most puzzling features of Soustov syenites is the coexistence of high initial $^{143}Nd/^{144}Nd$ and $^{87}Sr/^{86}Sr$ showing a weak positive correlation. If we accept that high initial $^{143}Nd/^{144}Nd$ represents a mantle feature, whereas high initial $^{87}Sr/^{86}Sr$ represents a crustal feature, then we are presented with the paradox that Soustov syenites are simultaneously enriched in both crustal and mantle components. An alternative explanation, however, might be that both features are linked to the percolation process, the enrichment in ^{87}Sr with respect to ^{86}Sr being caused by the destruction of biotite, as discussed in the above sections, and the enrichment in ^{143}Nd with respect to ^{144}Nd being caused by the differential leaching into the fluid of a mineral with high Sm/Nd that is at the same time significantly older than the metasomatic event. Our data on the tonalitic gneiss SUB-19 (Sm/Nd = 0.25) reveal that the range of Sm/Nd in co-existing minerals varies widely, from 0.16 in plagioclase to 0.36 in amphibole and 0.59 in apatite (Table 4). If, after a significant period of time from its formation, the rock is percolated by a metasomatic agent able to differentially leach the high-Sm/Nd minerals, the fluid would be progressively enriched in ^{143}Nd vs ^{144}Nd (and in LREE and $^{87}Sr/^{86}Sr$, as mentioned above). To model this mechanism, we have used Eq. 10 with the data from Tables 4 and 5, with the following results.

Among the minerals currently found in the SUB-19 gneiss, amphibole and apatite have the greatest influence on the enrichment in $^{143}Nd/^{144}Nd$ of the percolating fluid. When present, xenotime may cause even more dramatic effects. Monazite does not influence the Nd isotope ratio, since it has nearly the same Sm/Nd ratio as the whole rock. According to our calculations, the fluids are enriched in $^{143}Nd/^{144}Nd$ only when the age difference between protolith and metasomatism is greater than ~850 Ma (Fig. 9). Small differences in the age of the protolith can cause elevated differences in the $^{143}Nd/^{144}Nd$ of the fluid. Soustov syenites do not follow a single path of Sm vs $^{143}Nd/^{144}Nd$ enrichment, but plot between the paths corresponding to age differences of 900 Ma and 1000 Ma which is in concordance with the model for Sr isotopes (Fig. 10). The idea that the increased $^{143}Nd/^{144}Nd$ of the fluid may come from the

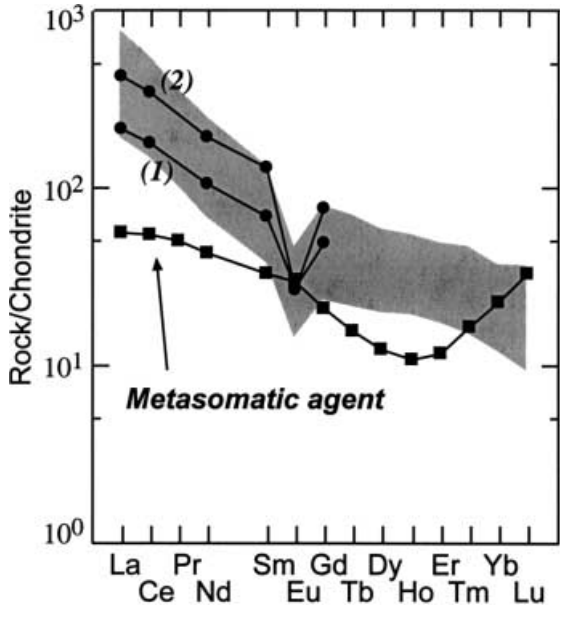

Fig. 9 Chondrite-normalized REE patterns of the metasomatic fluid at the beginning of the process and after percolating a gneiss mass (*1*) twice the mass of the solute and (*2*) four times the mass of the solute, as calculated from Eq. 10. The *shaded area* represents Soustov syenites. Note how the solute LREE patterns and abundances approach those of Soustov

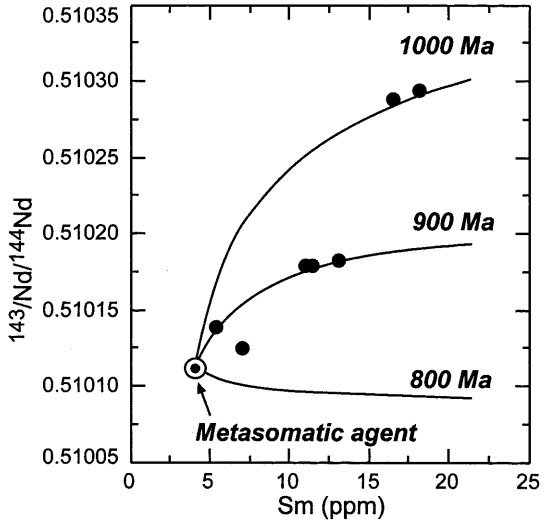

Fig. 10 Sm vs $^{143}Nd/^{144}Nd$ paths calculated from Eq. 10 for the various age differences between the metasomatic event and the percolated materials. Note the strong dependence on the age. Soustov syenites do not fit a single path, reflecting the heterogeneity of the protolith, which must have an age between 900 and 1,000 Ma

destruction of amphibole and apatite finds additional support from the excellent positive correlation between that parameter and such elements as MREE, Mg, Cr, Ni and P (Fig. 7).

A hypothesis for the origin of Soustov syenites

Numerical modeling of the infiltration metasomatism has revealed that a mantle-derived metasomatic agent derived from melts similar to Gremiakha-Vyrmes percolating through a ~1,000 Ma older gneissic protolith may acquire a chemical and isotopic composition similar to that of Soustov syenites. The metasomatic agent can, in principle, be an H_2O-CO_2 supercritical fluid or a melt. The elevated F, Cl, CO_2 and S contents of Soustov syenites (F and Cl in Table 1; CO_2 and S inferred from the abundance of accessory carbonates and sulfides) is a strong point in favour of the first alternative, since these elements, together with the alkalis and H_2O, are the most important components of the volatile phase of nephelinitic magmas (Bailey and Hampton 1990). Therefore, and taking into account that the dynamic properties of supercritical fluids are more favourable for infiltrating solid rocks that those of melts (Spera 1987), we suppose that the metasomatic agent was a supercritical fluid.

When released, the percentage of solute in the fluid must have been not less than 30% (Adam et al. 1997). As percolation progressed, the fluid would have dissolved silica and other components from the materials that fenitised, so that the composition of the solute would have changed from alkali halides, carbonates and sulfides to a silica-undersaturated alkaline melt. Both phases, hydrous fluid and silica-undersaturated alkaline melt, are completely miscible at moderate pressures if the temperature is higher than a critical value that, in the case of nepheline, has been estimated at 550 °C at 15 kb (Bureau and Keppler 1999). It therefore seems that, once the temperature dropped below the critical value, the fluid would have split into two components, a vapour phase with a small proportion of solute and a silicate melt that crystallised into the fluorite- and sodalite-bearing leucocratic syenites with a strong crustal imprint that form the Soustov intrusion.

Conclusions

The trace-element and isotope signatures of Soustov syenites reflect a strong crustal influence that cannot be accounted for by the bulk assimilation of host gneisses. We propose that Soustov melts derived from a metasomatic hydrous supercritical fluid, rich in alkali elements, F and Cl, that percolated through Archean tonalitic gneisses, fenitising them. The source of the fluid was a mantle-derived ultrabasic alkaline magma similar to those that formed Gremiakha-Vyrmes.

The mineralogical changes caused by reaction among the fluid and the minerals of the gneiss profoundly changed the fluid composition. The destruction of biotite, rich in radiogenic ^{87}Sr, coupled with the precipitation of minerals in which Sr is highly compatible, such as the feldspars, caused the increase in $^{87}Sr/^{86}Sr$ and the decrease in elemental Sr in the fluid. The destruction of biotite also caused the elevated Rb, Cs, Nb, low K/Rb, etc., contents of the fluid. The dissolution of monazite and allanite produced the elevated Th and LREE contents, negative Eu anomalies and low NdTh characteristic of Soustov melts.

The dissolution of minerals with elevated Sm/Nd such as hornblende and apatite caused the high $^{143}Nd/^{144}Nd$ in the fluid. The effect of biotite on Sr isotopes is perceptible when the age difference between the metasomatic event and the protolith is as low as 200 Ma, but in the case of Nd isotopes it requires at least 850 Ma. Numerical modelling with the expression derived for infiltration metasomatism, using the composition of a Gremiakha-Vyrmes pegmatite as the solute composition of the fluid, and the mode and the mineral trace-element and isotope composition of a TTG gneiss as representative of the protolith, indicates that the fluid would acquire a signature closely matching Soustov's if the gneiss age is ~2.9 Ga, which is probably close to its real age.

As the hydrous supercritical fluid percolated through the crust, its solute composition changed from alkali salts to a silica-undersaturated alkaline melt. When the fluid cooled to a temperature of ~600–550 °C, it reached the point at which vapour and melt are no longer miscible and it therefore split into two components, a vapour phase and a Cl- and F-rich silica-undersaturated silicate melt that crystallised to produce the sodalite-bearing syenites of Soustov. It should be emphasised that the fate of the percolating fluid does not have to be the unmixing at relatively low temperatures of a silica-undersaturated melt, but, depending on the PT regime and composition of the percolated crust, it may also cause local anatexis or mix in any way with pre-existing crustal melts, thus producing silica-oversaturated magmas. We tentatively suggest that the variability of $^{87}Sr/^{86}Sr_{initial}$ and the simultaneous occurrence of high $^{87}Sr/^{86}Sr_t$ and ϵNd_t occasionally found in peralkaline granitoids (Bennet et al. 1984; Eby 1990; Montero et al. 1998) might thereby be explained.

At the present level of knowledge, the crustal percolation model fits well with our observations, but it should be considered as a mere working hypothesis. To refine it, we need to understand in detail the behaviour of major and accessory minerals, as well as the chemical and isotopic exchanges involved during fenitisation. We hope that our current, ongoing research on some key examples from Kola might contribute to this objective.

Acknowledgements The authors are indebted to A. Vinogradov for his help with samples from Gremiakha-Vyrmes and fruitful discussions about the geology of Kola, and to K. Mengel and U. Kramm for their revisions of the manuscript. The help of Christine Laurin in improving the English is gratefully acknowledged. This work benefitted from the financial support of NATO

(grant 974904), the Spanish DGICYT (grant PB98-1345) and the Russian Foundation for Basic Research (grant 00-05-64229).

References

Adam J, Green TH, Sie SH, Ryan CG (1997) Trace element partitioning between aqueous fluids, silicate melts and minerals. Eur J Mineral 9: 569–584

Bailey DK, Hampton CM (1990) Volatiles in alkaline magmatism. Lithos 26: 157–165

Balashov YA (1996) The upper-mantle differentiation and mixing processes. New model on Sm.Nd isotopic data basis (in Russian). Dok Akad Nauk 347: 81–85

Batieva ID, Belkov IV, Kravchenko MP, Latyshev LN, Pushkariev YuD, Ulianenko NA (1983) The age of the Soustov alkaline massif, Kola Peninsula (in Russian). Dok Akad Nauk 270: 931–933

Bea F (1996) Residence of REE, Y, Th and U in granites and crustal protoliths; Implications for the chemistry of crustal melts. J Petrol 37: 521–552

Bea F, Montero P (1999) Behavior of accessory phases and redistribution of Zr, REE, Y, Th, and U during metamorphism and partial melting of metapelites in the lower crust: an example from the Kinzigite Formation of Ivrea-Verbano, NW Italy. Geochim Cosmochim Acta 63: 1133–1153

Bea F, Montero P, Stroh A, Baasner J (1996) Microanalysis of minerals by an Excimer UV-LA-ICP-MS system. Chem Geol 133: 145–156

Bea F, Montero P, Molina JF (1999) Mafic precursors, peraluminous granitoids, and late lamprophyres in the Avila batholith: a model for the generation of Variscan batholiths in Iberia. J Geol 107: 399–419

Bennet JN, Turner DC, Ike E, Bowden P (1984) The geology of some northern Nigerian anorogenic ring complexes. Overseas Geology and Mineral Resources n1/4 61, British Geological Survey, London

Bureau H, Keppler H (1999) Complete miscibility between silicate melts and hydrous fluids in the upper mantle: experimental evidence and geochemical implications. Earth Planet Sci Lett 165: 187–196

Eby N (1990) The A-type granitoids: a review of their occurrence and chemical characteristics and speculations on their petrogenesis. Lithos 26: 115–134

Govindaraju K, Potts PJ, Webb PC, Watson JS (1994) 1994 Report on Whin Sill Dolerite WS-E from England and Pitscurrie Micrograbbro PM-S from Scotland: assessment by one hundred and four international laboratories. Geostand Newsletters XVIII(2): 211–300

Green TH (1995) Significance of Nb/Ta as an indicator of geochemical processes in the crust-mantle system. Chem Geology 120: 347–359

Kober B (1986) Whole-grain evaporation for 207Pb/206Pb-age investigations on single zircons using a double filament thermal ionization source. Contrib Mineral Petrol 93: 482–490

Kresten P, Morogan V (1986) Fenitization at the Fen complex, southern Norway. Lithos 19: 27–42

Kukharenko AA, Bulakh AG, Ilyinsky GA, Shinkarev NF, Orlova M (1971) Metallogeny of alkaline rock series of the Eastern Baltic Shield (in Russian). Nedra, Leningrad

McKie D (1966) Fenitization. In: Tuttle OF, Gittins J (eds) Carbonatites. Wiley, New York, pp 261–295

McLemore VT, Modreski PJ (1990) Mineralogy and geochemistry of altered rocks associated with lemitar carbonatites, central New Mexico, USA. Lithos 26: 99–113

Mitrofanov FP, Pozhilenko VI, Smolkin VF, Arzamastsev AA, Yevzerov VYu, Lyubtsov VV, Nikolaeva SB, Fedotov ZhA (1995) Geology of the Kola Peninsula (Baltic Shield). Kola Science Center, Apatity

Montero P, Bea F (1998) Accurate determination of $^{87}Rb/^{86}Sr$ and $^{143}Sm/^{144}Nd$ ratios by inductively-coupled-plasma mass spectrometry in isotope geoscience: an alternative to isotope dilution analysis. Anal Chim Acta 358: 227–233

Montero P, Floor P, Corretge G (1998) The accumulation of rare-earth and high-field-strength elements in peralkaline granitic rocks: the Galineiro orthogneissic complex, northwestern Spain. Can Mineral 36: 683–700

Puskharev YD (1990) Megacycles in the evolution of the system crust – mantle (in Russian). Nauka, Leningrad

Savatenkov VM, Sulimov RB, Sergeev AV, Goncharov GN, Pushkarev YD (1998) Sm-Nd, Rb-Sr, and Pb-Pb isotope systematics of basic and ultrabasic rocks of Gremyakha-Vyrmes: the role of crust-mantle interaction in magma generation and ore-forming process (in Russian). Zap Vseross Mineral Ova 5: 15–25

Sindern S, Kramm U (2000) Volume characteristics and element transfer of fenite aureoles: a case study from the Iivaara alkaline complex, Finland. Lithos 51: 75–93

Spera J (1987) Dynamics of translithospheric migration of metasomatic fluid and alkaline magma. In: Menzies MA, Hawkesworth CJ (eds) Mantle metasomatism. Academic, London, pp 1–20

Stacey JS, Kramers JD (1975) Approximation of terrestrial lead isotope evolution by a two-stage model. Earth Planet Sci Letters 26: 207–221